

# Diagnosing the sensitivity of grounding line flux to changes in sub-ice shelf melting

Tong Zhang, Stephen Price, Matthew Hoffman, Xylar Asay-Davis

*Fluid Dynamics and Solid Mechanics Group, Los Alamos National Laboratory, New Mexico, United States, 87545*

*Correspondence: Tong Zhang <tzhang@lanl.gov>*

**ABSTRACT.** Motivated by previous work using ice flow models to quantify ice shelf buttressing and its impacts on the flux of ice across the grounding line (e.g., ??), we seek a better physical understanding for how ice dynamics link small ice thickness perturbations, via changes in sub-ice shelf melting, to changes in ice shelf buttressing and ice flux across the grounding line. More specifically, we seek to define one or more ice shelf buttressing “metrics” that are readily calculated from standard ice sheet model outputs and are simultaneously informative for diagnosing the sensitivity of grounding line flux to ice thickness at specific locations on an ice shelf. By studying the ice dynamics for both idealized (MISMIP+) and realistic (Larsen C) ice shelves, we find that the first principle stress at perturbation locations is the best overall metric for linking local changes in ice shelf dynamics with changes in the integrated grounding line flux. Unfortunately, this metric only shows a robust relationship with the integrated grounding line flux for regions near the center of an ice shelf; for points too near the grounding line or too near the calving front, no clear relationship exists between any of the readily calculable metrics explored here and changes in grounding line flux. This motivates our exploration of an adjoint-based method for defining grounding line flux sensitivity to local changes in ice shelf geometry. Using the same idealized

and realistic test cases, we demonstrate that this method is equivalent to the sensitivity analysis of (?) but requires only a single model adjoint solve. Thus we suggest that the adjoint-based method can provide a model run-time means of analyzing grounding line flux sensitivity to changes in sub-ice shelf melting.

## INTRODUCTION

Marine ice sheets like West Antarctica (and to a lesser extent, portions of East Antarctica) are grounded below sea level and their bedrock would remain so even after full isostatic rebound [REFS]. This and the fact that ice sheets generally thicken inland lead to a geometric configuration that is unstable; a small increase in flux at the grounding line thins the ice there, leading to floatation, a retreat of the grounding line into deeper water, further increases in flux (due to thicker ice), and further thinning and grounding line retreat. This theoretical “marine ice sheet instability” mechanism [Mercer,Schoof1] is supported by idealized [Schoof2,MISMIP+?] and realistic ice sheet modeling [Gudmundson,others?] experiments and some studies [Rignot, Joughin] argue that such an instability is currently under way along outlet glaciers of Antarctica’s Amundsen Sea Embayment (ASE). The relevant perturbation for grounding line retreat in the ASE is thought to be intrusions of relatively warm, intermediate depth ocean waters onto the continental shelves [ref to recent review papers in Oceanography? or other recent reviews?], which have reduced the thickness and extent of marginal ice shelves via increased submarine melting [REFS]. These reductions are critical because fringing ice shelves restrict the flux of ice across their grounding lines farther upstream – the so-called “buttressing” affect of ice shelves [gudmundssonOLD,gudmundsson2013,GudmundssonAndDeRydtPaperOnLarsenC?] – which makes them a critical control on ice flux from Antarctica to the ocean.

On ice shelves, gradients in hydrostatic pressure are balanced by the primarily extensional flow of ice towards the calving front (?) [add a more basic ref, like Paterson, Van der Veen?] and, in theory, a one-dimensional ice shelf provides no buttressing (??). *SP: I wonder if this requires a monotonic decrease in ice shelf thickness though?* For realistic, three-dimensional ice shelves however, buttressing results from three main sources: 1) compressive ice flow 2) lateral shear, and 3) “hoop” stress (?). *For completeness, we should probably briefly describe how each of these contributes to buttressing rather than assume people already know (?). The first two are easy. I’m not sure about the 3rd.* Due to the complex geometries,

kinematics, and dynamics of real ice shelves, an understanding of the specific processes and locations that control ice shelf buttressing is far from straightforward.

Several recent studies apply whole-Antarctic ice sheet models optimized to present-day observations towards improving our understanding for how Antarctica ice shelves limit flux across the grounding line and, by extension, ice dynamics farther inland. ? ... *add a few more details on their methods here?* ... to identify regions of the ice shelves that are dynamically “passive”, such that increased submarine melting, or even complete removal of ice in these areas should not significantly alter local or regional ice dynamics or the flux of ice upstream. ? used perturbation experiments to link small, localized decreases in ice shelf thickness to changes in integrated grounding line flux (GLF), thereby providing a map of GLF sensitivity to local increases in submarine melt rates.

Motivated by these (and other? which?) studies, we build on and extend the methods and analysis of Furst et al. and Reese et al. in order to make progress towards answering the following questions: (1) How do local and regional changes in ice shelf geometry affect distal changes in GLF? (2) Can local or regional ice shelf dynamics explain GLF sensitivity to local or regional changes in ice shelf thickness? (3) Can we derive and define new tools and analyses for understanding how observed or modeled spatial patterns in submarine melting influence GLF and, by extension, project how changes in submarine melt pattern and magnitude will impact GLF in the future?

Below, we first provide a brief description of the ice sheet model used in our study. We follow with a description of the model experiments and a discussion of the experimental results and their interpretation. We then demonstrate and discuss the pros and cons of a number of possible metrics for quantifying GLF sensitivity to changes in submarine melt. Based on limitations in all metrics explored here, we conclude by proposing and demonstrating an adjoint-based calculation that provides a sensitivity map analogous to that from the ? perturbation experiments but at the cost of a single model adjoint solve.

## MODEL DESCRIPTION

*SP: I built out this section a bit more. We can reduce later on if needed but it seemed a bit too thin. Note that this is mostly copied and lightly edited from the MALI paper, so we’ll have to look over carefully and make sure it doesn’t end up looking self-plagiarized.* We use the MPAS-Albany Land Ice model (MALI; ?), which solves the three-dimensional, first-order approximation to the Stokes momentum balance for ice

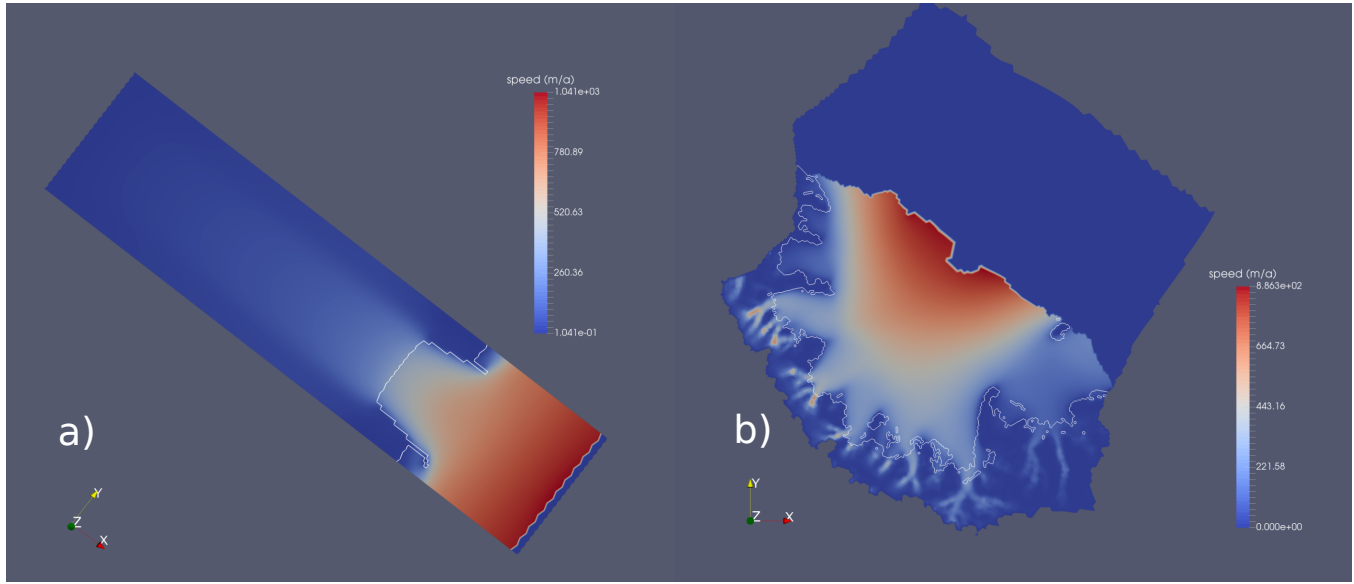


**Fig. 1.** Plan view of steady-state surface ice speeds for MISMP+ (a) and present-day surface ice speed for Larsen C ice shelf (b). The white curves show the grounding lines.

flow<sup>1</sup>. Using the notation of  $\dot{\epsilon}$  and  $\mu_e$  this can be expressed as,

$$\begin{cases} -\nabla \cdot (2\mu_e \dot{\epsilon}_1) + \rho_i g \frac{\partial s}{\partial x} = 0, \\ -\nabla \cdot (2\mu_e \dot{\epsilon}_2) + \rho_i g \frac{\partial s}{\partial y} = 0, \end{cases} \quad (1)$$

where  $x$  and  $y$  are the horizontal coordinate vectors in a Cartesian reference frame,  $s(x, y)$  is the ice surface elevation,  $\rho_i$  represents the ice density,  $g$  the acceleration due to gravity, and  $\dot{\epsilon}_{1,2}$  are the two dimensional strain rate vectors given by

$$\dot{\epsilon}_1 = \begin{pmatrix} 2\dot{\epsilon}_{xx} + \dot{\epsilon}_{yy}, & \dot{\epsilon}_{xy}, & \dot{\epsilon}_{xz} \end{pmatrix}^T, \quad (2)$$

and

$$\dot{\epsilon}_2 = \begin{pmatrix} \dot{\epsilon}_{xy}, & \dot{\epsilon}_{xx} + 2\dot{\epsilon}_{yy}, & \dot{\epsilon}_{yz} \end{pmatrix}^T. \quad (3)$$

The “effective” ice viscosity,  $\mu_e$  in Equation ??, is given by

$$\mu_e = \gamma A^{-\frac{1}{n}} \dot{\epsilon}_e^{\frac{1-n}{n}}, \quad (4)$$

where  $\gamma$  is an ice stiffness factor,  $A$  is a temperature-dependent rate factor,  $n = 3$  is the power-law exponent, and the effective strain rate,  $\dot{\epsilon}_e$ , is defined as

$$\dot{\epsilon}_e \equiv (\dot{\epsilon}_{xx}^2 + \dot{\epsilon}_{yy}^2 + \dot{\epsilon}_{xx}\dot{\epsilon}_{yy} + \dot{\epsilon}_{xy}^2 + \dot{\epsilon}_{xz}^2 + \dot{\epsilon}_{yz}^2)^{\frac{1}{2}}. \quad (5)$$

<sup>1</sup>See ? for a full description of the Stokes momentum balance for ice flow and its lower-order approximations.

90 Gradients in the horizontal velocity components,  $u$  and  $v$ , contribute to the individual strain rate terms in  
 91 Equation ?? and are given by

$$\dot{\epsilon}_{xx} = \frac{\partial u}{\partial x}, \quad \dot{\epsilon}_{yy} = \frac{\partial v}{\partial y}, \quad \dot{\epsilon}_{xy} = \frac{1}{2} \left( \frac{\partial u}{\partial y} + \frac{\partial v}{\partial x} \right), \quad \dot{\epsilon}_{xz} = \frac{1}{2} \frac{\partial u}{\partial z}, \quad \text{and} \quad \dot{\epsilon}_{yz} = \frac{1}{2} \frac{\partial v}{\partial z}. \quad (6)$$

92 A stress free upper surface is enforced through

$$\dot{\epsilon}_1 \cdot \mathbf{n} = \dot{\epsilon}_2 \cdot \mathbf{n} = 0, \quad (7)$$

93 where  $\mathbf{n}$  is the outward pointing normal vector at the ice sheet upper surface,  $z = s(x, y)$ . The lower surface  
 94 is allowed to slide according to the continuity of basal tractions,

$$2\mu_e \dot{\epsilon}_1 \cdot \mathbf{n} + \beta u = 0, \quad 2\mu \dot{\epsilon}_2 \cdot \mathbf{n} + \beta v = 0, \quad (8)$$

95 where  $\beta$  is a spatially variable, linear-friction coefficient. On lateral boundaries in contact with the ocean,  
 96 the portion of the boundary above sea level is stress free while the portion below sea level feels the ocean  
 97 hydrostatic pressure according to

$$2\mu_e (\dot{\epsilon}_1 \cdot \mathbf{n}, \dot{\epsilon}_2 \cdot \mathbf{n}, 0)^T - \rho_o g(s - z)\mathbf{n} = \rho_o g \max(z, 0)\mathbf{n}, \quad (9)$$

98 where  $\rho_o$  represents the density of ocean water and  $\mathbf{n}$  the outward pointing normal vector to the lateral  
 99 boundary (i.e., parallel to the  $(x, y)$  plane).

100 A more complete description of the full MALI model, including the implementations for mass and energy  
 101 conservation, can be found in ?. Additional details about the Albany momentum balance solver can be  
 102 found in ??.

103 Here, we apply MALI to experiments on both idealized and realistic marine-ice sheet geometries. For  
 104 our idealized domain and model state, we start from the equilibrium initial conditions for the MISIP+  
 105 experiments, as described in ? and Cornford and others (MISIP+ papers). The model mesh is spatially  
 106 uniform at 2 km resolution. For our realistic domain, we use Antarctica's Larsen C ice shelf and its  
 107 upstream catchment area. The model state is based on the optimization of the ice stiffness ( $\gamma$  in Equation  
 108 ??) and basal friction ( $\beta$  in Equation ??) coefficients to match present-day velocities (?) using adjoint-based  
 109 methods discussed in ? and ?. The domain geometry is based on BEDMAP2 (?) and ice temperatures,  
 110 which are held fixed for this study, are based on ?. Mesh resolution coarsens to 20 km in the ice sheet  
 111 interior and is no greater than 6 km within the ice shelf *This seems coarse to me ... don't we go to finer*  
 112 *resolution, e.g. 2 km, near the g.l.?* Following optimization to present-day velocities, the model is relaxed

using a 100 year forward run and it is this initial condition from which the experiments discussed below are conducted. Both the MISMIP+ and Larsen C experiments use 10 vertical layers that are finest near the bed and coarsen towards the surface (4% and 23% of the total thickness, respectively). The grounding line position is determined from hydrostatic equilibrium and a sub-element parameterization analogous to method SEP3 from ? is used to define basal friction coefficient values at the grounding line.

## PERTURBATION EXPERIMENTS

To explore the sensitivity of changes in GLF to small changes in ice shelf thickness, we conduct a number of perturbation experiments analagous to those of ?. Using diagnostic model solutions, we first study the instantaneous response of GLF for the idealized geometry and initial state provided by the MISMIP+ experiment (?). We then conduct a similar study but using a realistic configuration and initial state for Antarctica’s Larsen C ice shelf.

Our experiments are conducted in a manner similar to those of ?. We perturb the coupled ice sheet-shelf system by decreasing the ice thickness uniformly by 1 m over square grid “boxes” covering the base of the ice shelves, after which we examine the instantaneous impact on kinematics and dynamics (discussed further below). For MISMIP+, the uniform, 2 km mesh implies that grid cell centers naturally align with these boxes. For the Larsen C ice shelf, horizontal mesh resolution is spatially variable and we assign each grid cell to fall within one and only one box based on its location. For MISMIP+, we use 2×2 km square boxes that are also the real cell size. For Larsen C, we only use 20×20 km square boxes (i.e., as in ?). Lastly, for the MISMIP+ 2 km experiments we note that, in order to save on computing costs, we only perturb the region of the ice shelf for which  $x < 530$  km (the area over which the ice shelf is likely laterally buttressed) and  $y > 40$  km (one half of the ice shelf due to the symmetry about the centerline).

Similar to ?, we define a GLF response number

$$N_r = \left( \frac{R}{P} \right)^k, \quad (10)$$

where  $R$  is the ice flux change integrated along the entire grounding line,  $P$  is the mass associated with a single grid box perturbation (e.g., 2 km×2 km ×0.001 km for the MISMIP+ perturbation experiments) and  $k$  is a power-law index that allows for the possiblity of a nonlinear relationship between ice shelf buttressing and the change in GLF (see also ?). Here, we use  $k = 1/n$  ( $n = 3$ ).

Despite the existence of many different factors (ice flow directions, horizontal gradients of ice shelf geometry, stress fields, strain-rate fields, perturbation locations, etc), we here mainly present the results

of the stress fields and the distances between perturbations and GL, as they appears to correlate more closely to the sensitivity of GL flux change to ice shelf perturbations. Similar to ? (Eqn ??), we calculate buttressing numbers ( $N_b$ ) as follows,

$$N_b = 1 - \frac{\sigma_{nn}}{N_0}, \quad (11)$$

where  $N_0$  is the vertically integrated ocean pressure ( $N_0 = 0.5(1 - \rho_i/\rho_w)gH$ ).  $\rho_i$  (910 kg m<sup>3</sup>) and  $\rho_w$  (1028 kg m<sup>3</sup>) are the density of ice and ocean water, respectively.  $\sigma_{nn}$  is the normal stress along certain horizontal direction.

## RESULTS AND DISCUSSIONS

### Linear relationship between buttressing ( $N_b$ ) and GL flux responses ( $N_r$ )

The decrease of ice shelf buttressing tends to induce the increase of GLF (?). Therefore, the highly buttressed regions are in general more sensitive to sub-ice shelf melting for marine ice sheet dynamics. It is thus useful to understand more quantitatively the relationship between the buttressing “strength” (number) and the GLF changes. Can we predict the changes of GLF simply by the buttressing number ( $N_b$ )? By calculating the buttressing number ( $N_b$ ) along the first principle stress ( $\sigma_{p1}$ ) direction, we can see very weak  $N_b$ - $N_r$  correlations from the results of all perturbation experiments (Fig ??b). However, if we do not consider the perturbation points that are weakly buttressed ( $x > 480$  km; near the open shelf region) and are close to GL (the minimum distances between GL and perturbation points are greater than 5 km), we can clearly see a strong linear  $N_b$ - $N_r$  regression (Fig ??c). A similar strong linearity can also be found if we apply a different filtering approach using the ice thickness gradient field (Fig ??a), i.e., we keep the perturbation points that have thickness gradients smaller than 0.0007 (Fig ??d). This nonlinearity feature is likely caused by the intensive shearing and complex ice flow mechanics near GL (a strong transition zone from relatively slow grounded ice flow to fast extensively floating ice flow). We can again see this non-linearity region in our adjoint sensitivity experiments (Fig. ?? in section “Adjoint sensitivity”).

### The buttressing directions

According to Equation ??, the buttressing number  $N_b$  is computed by the normal stress ( $\sigma_{nn}$ ) along specific directions. Therefore, the buttressing at certain perturbation points can be various for different directions we apply. In ? the buttressing along two significant directions (flow and second principle stress ( $\sigma_{p2}$ )) was analyzed, and found that the  $\sigma_{p2}$  buttressing, which points to the most compression direction, has the

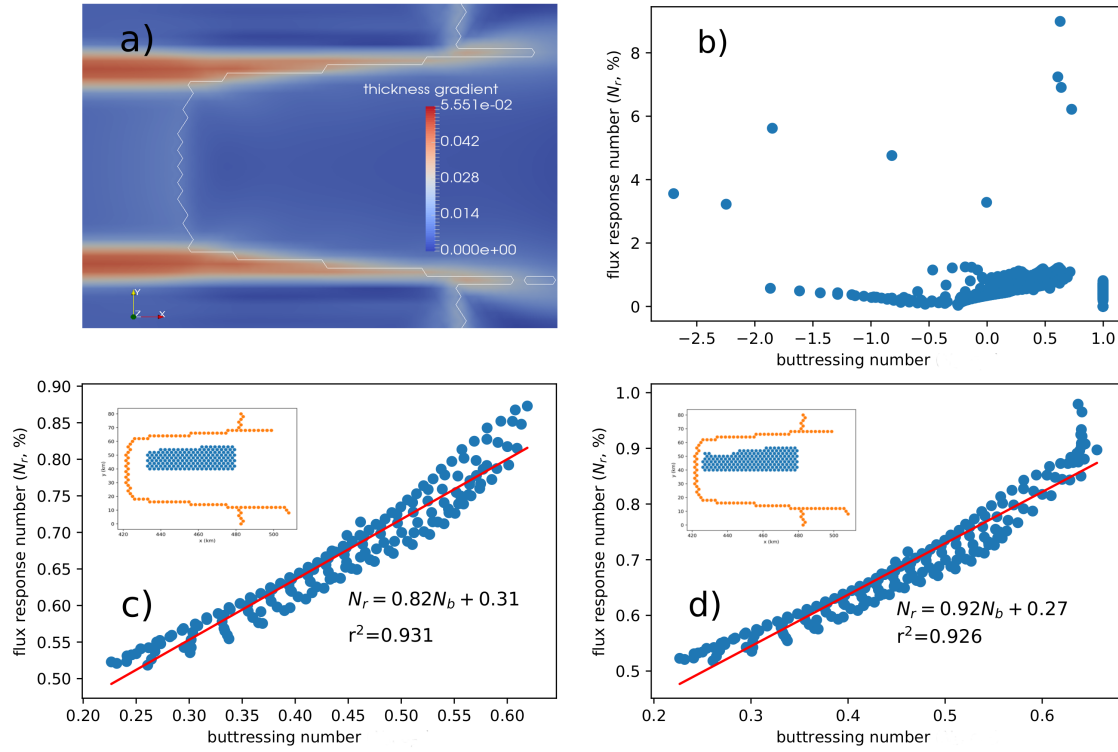


**Fig. 2.** (a) The magnitude of ice thickness gradient around GL (white curve) for the steady-state MISMIP+ geometry; (b) The relationship of  $N_b$ - $N_r$  for all perturbation points; (c) The relationship of  $N_b$ - $N_r$  for perturbation points that are  $>10$  km away from GL; (d) The relationship of  $N_b$ - $N_r$  for perturbation points with thickness gradient  $< 7 \times 10^{-3}$ . The red (blue) dots in the insets are GL (perturbation) cells.

maximum impacts on the “passive” ice shelf regions. Here we get the correlation numbers ( $r^2$ ) between  $N_r$  and  $N_b$  for different directions with respect to the first principle stress and flow direction, respectively (Fig ??). Differently, we find that  $N_b$  along the  $\sigma_{p1}$  direction shows the best regression performance, whereas the  $\sigma_{p2}$  appears to show the weakest correlations to  $N_r$ . This can be further testified by looking at the angle differences between  $\sigma_{p1}$  and flow directions ( $\Delta\phi = \phi_{flow} - \phi_{\sigma_{p1}}$ ). From Figure ??b, we see that for around 50% of the perturbation points, their flow directions are around 30–50 degree more than the  $\sigma_{p1}$  directions, which is consistent with the phase differences in Figure ??a. If we add around 40 degree on top of the flow direction (blue curve), the new direction will be likely aligned closely with the  $\sigma_{p2}$  direction, which is consequently pointing to the smallest  $r^2$  number for the  $\sigma_{p1}$  (red) curve. This indicates that the



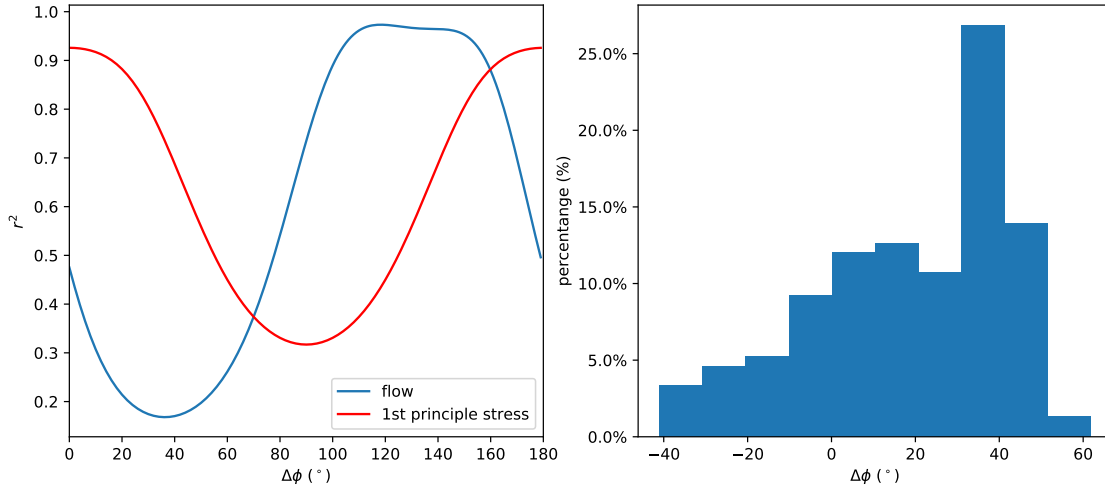


**Fig. 3.** (a) The  $N_b$ - $N_r$  regression coefficients for each direction rotated anti-clock-wisely from the  $\sigma_{p1}$  (red) and flow direction (blue); (b) The histogram of the angle differences between flow and  $\sigma_{p1}$  directions. The perturbation points we apply here are the same as in Figure ??d.

177 local maximum buttressing relating to  $\sigma_{p2}$  is unnecessarily corresponding to the integrated instantaneous  
 178 GLF responses.

### 179 Possible controlling factors

180 Further clues of the impacts from different chosen directions can be found in Figure ?. We analyzed the  
 181 number of maximum (light red) and minimum (blue) velocity changes around each perturbation point for  
 182 the cases using flow (Fig ??a) and  $\sigma_{p1}$  directions (Fig ??b). Figure ??a and c contain all perturbation  
 183 points while Figures ??b and d only include the filtered perturbation points as in Figure ??d. For the  
 184 flow direction results, most of the maximum (minimum) velocity change events occur along the flow (120  
 185 degree) direction. The  $\sigma_{p1}$  direction results are more spread than of the flow direction results. However, it is  
 186 still clear that most of the maximum (minimum) velocity change events are aligned near the first (second)  
 187 principle stress direction, a supporting evidence for our previous findings.

188 Another evidence is the standard deviation of the differences between the relative changes of stress and  
 189 velocity ( $\Psi$ ) along GL (Fig ??).

$$\Psi = \frac{\sigma_p - \sigma_c}{\sigma_c} - \frac{u_p - u_c}{u_c}, \quad (12)$$

190 where the subscripts  $p$  and  $c$  denote perturbation experiments and ctrl runs.  $\sigma$  and  $u$  denote the stress  
 191 component and ice velocity, respectively. This is a measure of the consistency of velocity and stress variances

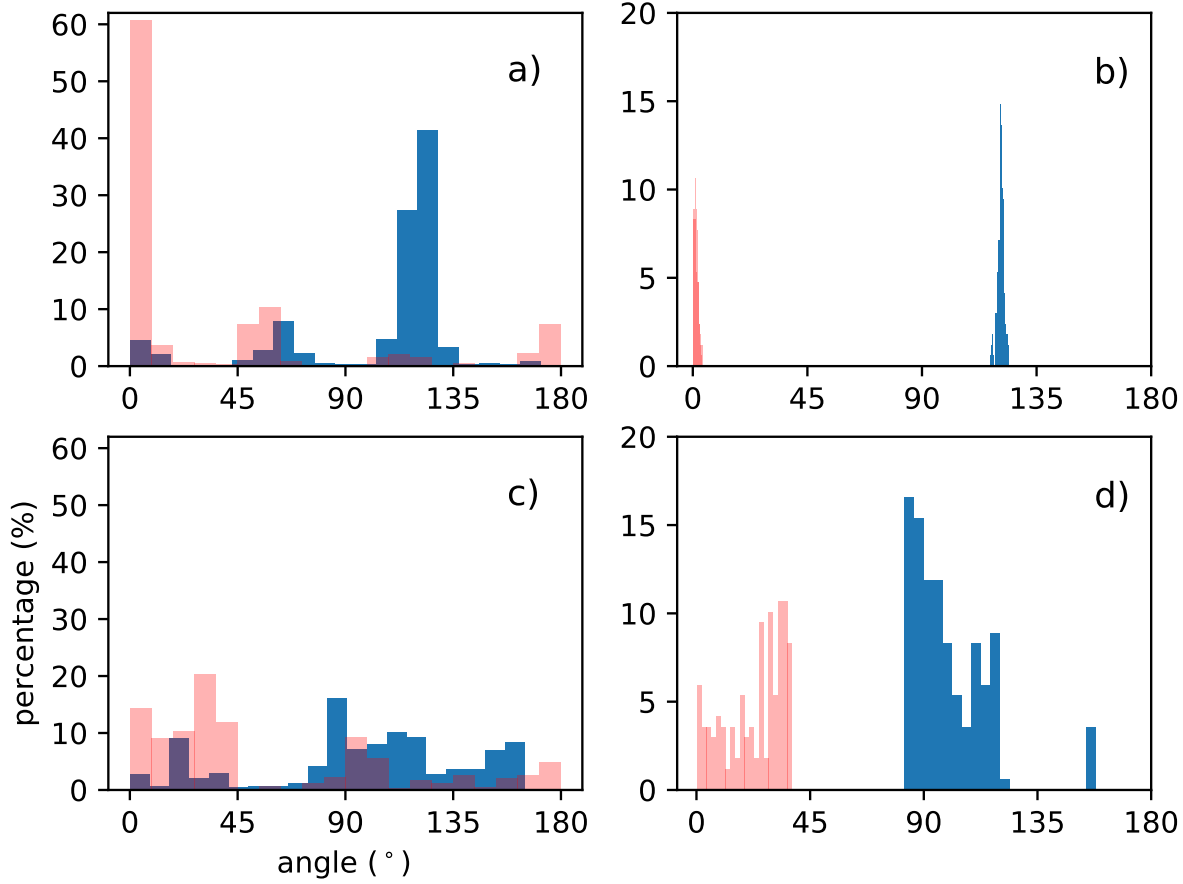


**Fig. 4.** Histograms of the frequency of the neighboring maximum (red) and minimum (blue) velocity change around all perturbation points (a and c) and around the same selected perturbation points (b and d) as Figure ??d (**TZ:** this figure still needs double check!)

192 along GL under certain perturbation experiments. Here we choose  $\sigma_{p1}$  and  $\sigma_{p2}$  for instances, i.e., we set  $\sigma$   
 193 in Equation ?? to  $\sigma_{p1}$  and  $\sigma_{p2}$ . Overall, the  $\sigma_{p1}$  case (Fig ??a) shows smaller standard deviations, especially  
 194 for perturbation points close to GL, than the  $\sigma_{p2}$  case (Fig ??b). This possibly indicates that GLF are  
 195 more relevant to the changes of  $\sigma_{p1}$  along GL, compared to the  $\sigma_{p2}$  case, which can be clearly found if we  
 196 look at some specific perturbation example as shown in Figure ??.

197 One of the possible reasons for us seeing such direction-dependent correlations might be due to the  
 198 perturbation propagation features on ice shelves. The energy of perturbation propagates with the group  
 199 velocity if we decompose it using Fourier transform. A similar example can be found in (?). Using very  
 200 simplified geometry ? analyzed the propagation of basal perturbation to glacier surface and found that the  
 201 direction of group velocity is aligned closely with the main flow. The existence of preferred propagation

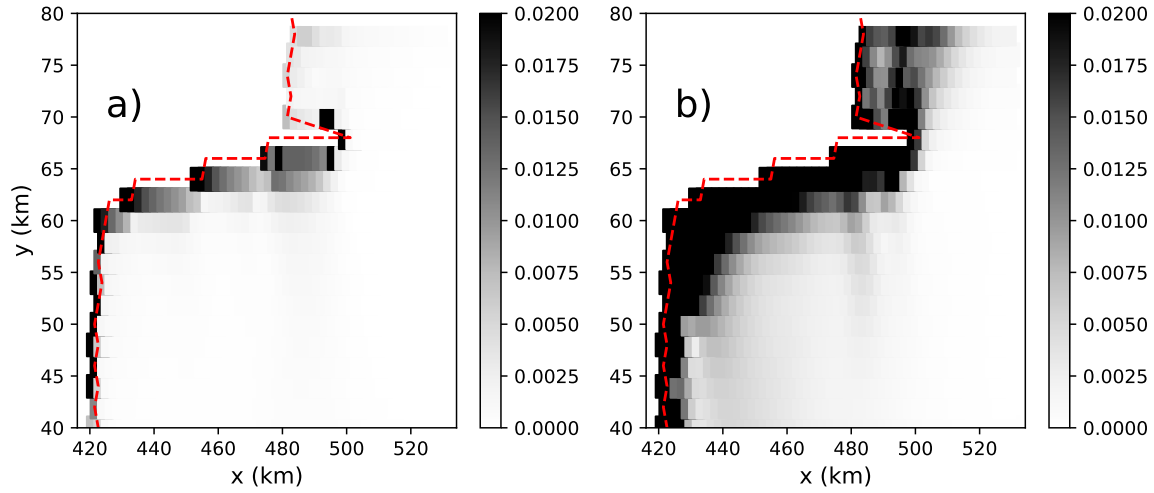


**Fig. 5.** The standard deviations of  $\Psi$  along GL for each perturbation point for the case of  $\sigma_{p1}$  (a) and  $\sigma_{p2}$  (b).

202 direction for the perturbations can possibly lead to our findings that favor the first principle stresses (**TZ:**  
 203 **I am still not able to explain why it's exactly the first principle stress direction :(**).

#### 204 Application on Larsen C ice shelf

205 To validate if there are the same  $N_b$ - $N_r$  patterns as in the MISMP+ case for realistic ice shelves, we apply  
 206 the same analysis processes as above to the Larsen C ice shelf. Because the mesh resolution varies from GL  
 207 to calving front, we apply  $20 \text{ km} \times 20 \text{ km}$  square boxes to the perturbation experiments and adjust the

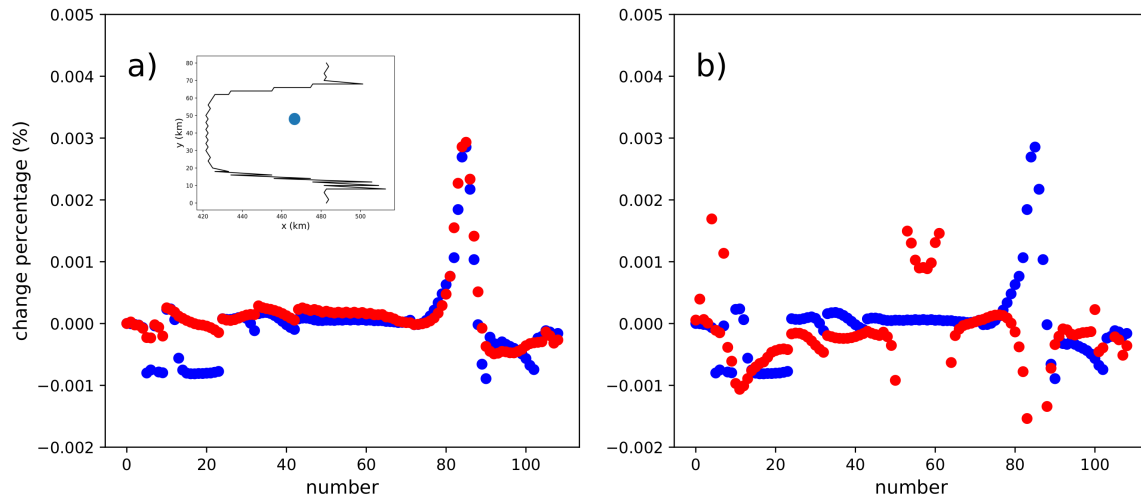


**Fig. 6.** An example showing the relationship of the change of velocity (blue) with  $\sigma_{p1}$  (red; a) and  $\sigma_{p2}$  (red; b). The  $x$ -axis shows the cell number along GL. The inset shows the perturbation location.

box areas by counting actual cell numbers that each box includes. In addition, to account for the complex geometry (GL shape and ice rises) of Larsen C ice shelf, we use two different perturbation sets with and without including near-GL boxes for investigating further the nonlinearity feature we observe in the above MISMIP+ section.

From Figure ??a, we can see similar  $N_b$ - $N_r$  correlation patterns to that of the MISMIP+ case. Along the  $\sigma_{p1}$  direction we have the best  $N_b$ - $N_r$  correlations ( $\Delta\phi = 0$ , red curve), whereas along the  $\sigma_{p2}$  ( $\Delta\phi = 90$ , red curve) direction they are the most insignificant. The phase difference between the  $\sigma_{p1}$  and flow direction results can also be partially explained by their respective angle differences. In Figure ??b we can find the angles of flow directions are mostly around 90–100 degrees larger than that of the  $\sigma_{p1}$  directions. This is a bit biased than the around 70 degree difference in Figure ??a. However, considering the stress values (and thus  $N_b$ ) for each perturbation box are averaged over multiple cells, we argue this difference is probably an acceptable error during our calculation.

By including some near-GL perturbation boxes (Fig. ??c and d), the  $r^2$  features get disturbed as well. Although the angle differences between the flow and  $\sigma_{p1}$  directions are still mostly near 90 degree, there are no longer clear patterns in the phase differences for the corresponding  $r^2$  curves. In addition, the  $\sigma_{p1}$  directions are also no longer indicating the best  $r^2$  correlations. However, the directions along  $\sigma_{p2}$  appears to still pointing to the weakest  $N_b$ - $N_r$  correlations, despite the overall much smaller  $r^2$  values in this case.

## Impacts of near-GL perturbations

For the near-GL perturbations, it is hard to find similar linear regression relationship as discussed above. Alternatively, they are largely controlled by the distance between GL and perturbation points and also by the geometric features around them. As the perturbation decays over distance (?), the neighboring GL cells of those near-GL perturbations will relatively easily detect the perturbation energy. This can be verified by looking at the standard deviations of GL velocity change due to each perturbation (Fig ??). For perturbations close to GL, their corresponding GL flux changes are in general confined to local regions, while in the remote GL sections the velocity changes are often negligible, resulting in large standard deviations. This can possibly cause spatial heterogeneity of GL retreating if the sub-shelf melting is very close to GL and is heavily local confined.

The propagation of perturbation can also be impacted by the spatial GL geometry, e.g., they can be blocked by the local GL. For example, the perturbation at around  $x = 480$  km and  $y = 65$  km in Figure ??a can not directly impact the ice flow on the other side of the grounded peninsula (e.g.,  $x=485$  km,

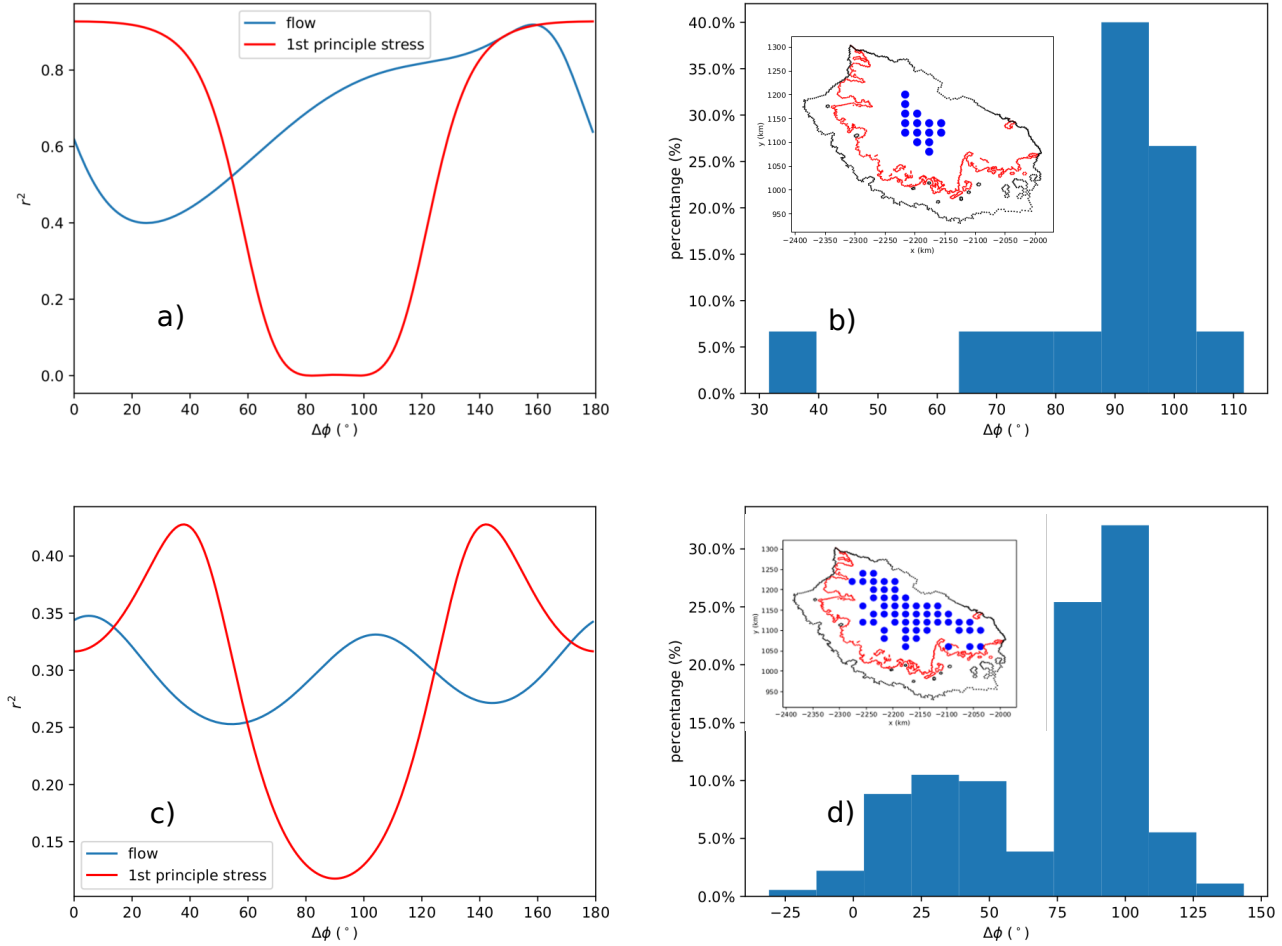


**Fig. 7.** (a, c) The  $N_b$ - $N_r$  regression coefficients for each direction rotated anti-clock-wisely from the  $\sigma_{p1}$  (red) and flow direction (blue); (b, d) The histogram of the angle differences between flow and  $\sigma_{p1}$  directions. The insets in b) and d) show the perturbation boxes (blue circles).

238  $y=70\text{km}$ ) in the same way as for it's neighboring cells. This is one of the major factors that complicate  
 239 our diagnostic analysis for real ice shelves (for example, Larsen C) containing complex GL shapes and  
 240 geometries.

## 241 Adjoint sensitivity

242 Need helps from Steve and Mauro!

## 243 CONCLUSIONS

244 From this study we find that the sensitivity of grounding line (GL) flux to melt perturbations beneath  
 245 ice shelves appears to be linearly related to the buttressing number for certain stress field of the ice flow

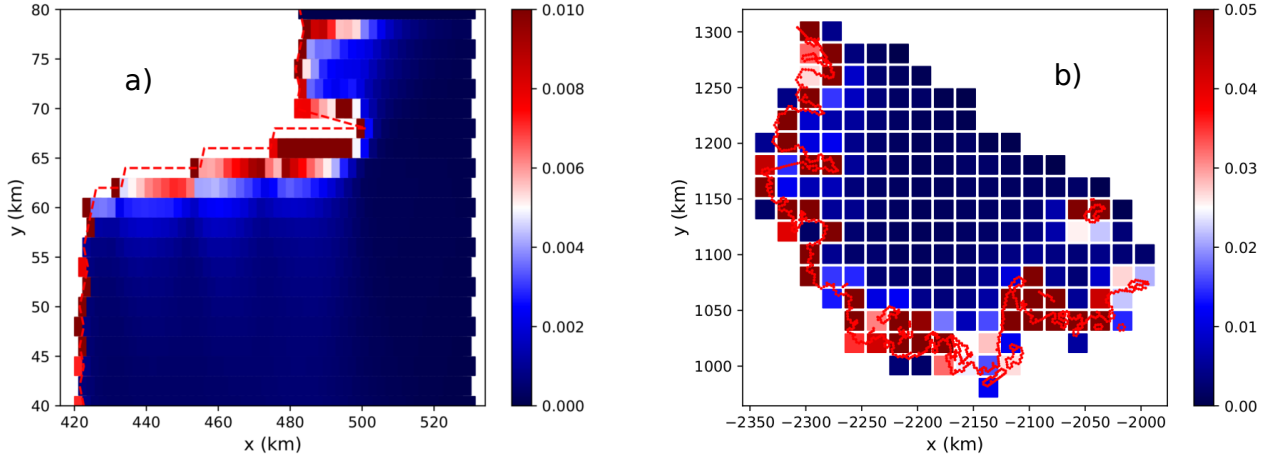


**Fig. 8.** Standard deviation of velocity change along GL for each perturbation point for the MISMP+ (a) and Larsen C (b) experiment. The red dashed lines (points) are the GLs for MISMP+ (a) and Larsen C (b) .

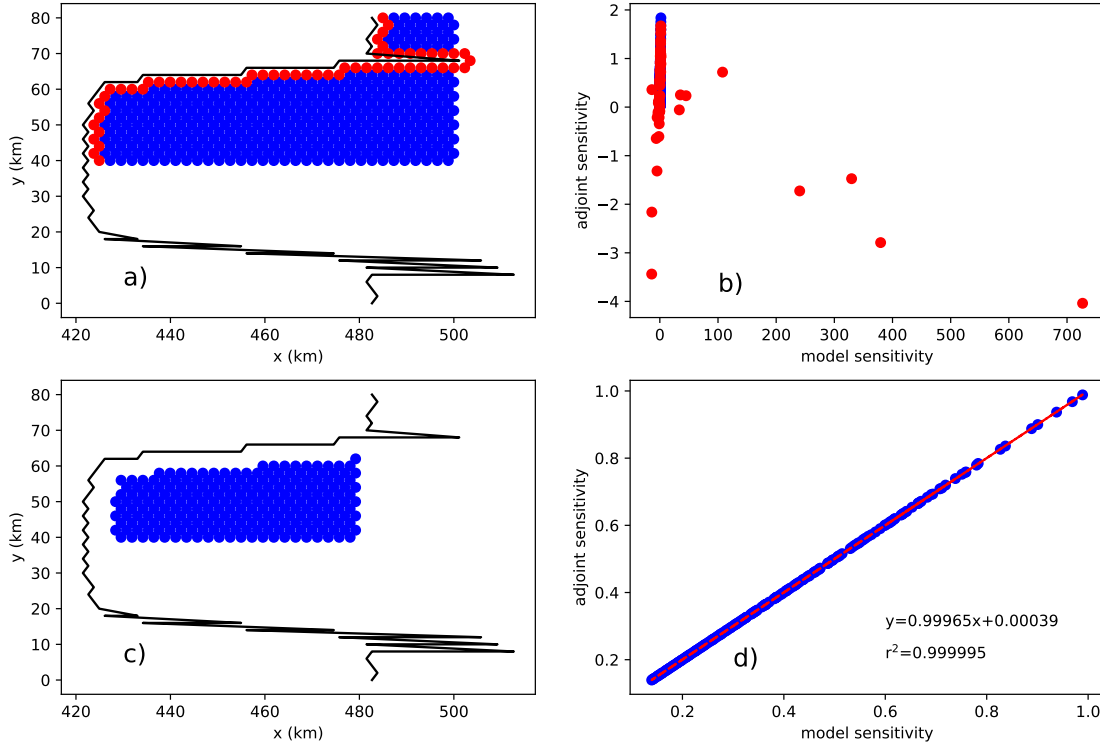


**Fig. 9.** (a, c) Perturbation points. The red points indicate near-GL (<2 km) points. GL is the black curve; (b, d) Model sensitivity by perturbation experiments versus adjoint sensitivity. The red dashed curve shows their linear regression.

regime when the perturbations are located near the center of ice shelves. We can divide an ice shelf into three different geometric regions: 1) near GL where the shear margins dominate; 2) near the calving fronts where ice can be considered as “passive” and 3) the central regions of ice shelf. Though it is ambiguous to indentify the boundaries of those three sub-regions, we find that both the shear margins and passive ice regions show very weak linear connections to GL flux changes. The shear margins are strongly impacted by the upstream grounded stream flows and the passive ice shelf basically has negligible contribution to GL dynamics.

The buttressing of ice shelf resists ice flows from upstream. The maximum buttressing number (calculated from the second principle stress  $\sigma_{p2}$ ) is a commonly used metric to quantify the buttressing effects of ice shelf, doesn’t show clear correlations to the changes of GL flux. Among many possible factors we find that the distance away from perturbation locations may be a critical control for perturbation propagation across ice shelves, which is important for understanding the relationships between the stress field of the ice shelf and the GL flux changes. The GL ice speed changes may be more correlated to the changes of the first principle stress ( $\sigma_{p1}$ ) and normal stress along flow ( $\sigma_f$ ) than other stress components, for example, the second principle stress ( $\sigma_{p2}$ ) and the shear stress ( $\sigma_s$ ), indicating that the stress component ( $\sigma_{p2}$ ) that contribute significantly to buttressing is not necessarily related to the propagation of buttressing.

The linear  $N_b$ - $N_r$  relationships presented in this study are based on small (1 m) thickness perturbations. However, it’s still unclear if they can stand for large melts at the bottom of ice shelves (**Perhaps we also need to do large perturbation experiments?**). Despite the progress we have made in this study, we suggest to apply a fully-developed perturbation propagation model for further understanding the physics of GL flux changes under ocean forcings.

## ACKNOWLEDGEMENT

## APPENDIX